CHALMERS
UNIVERSITY OF TECHNOLOGY

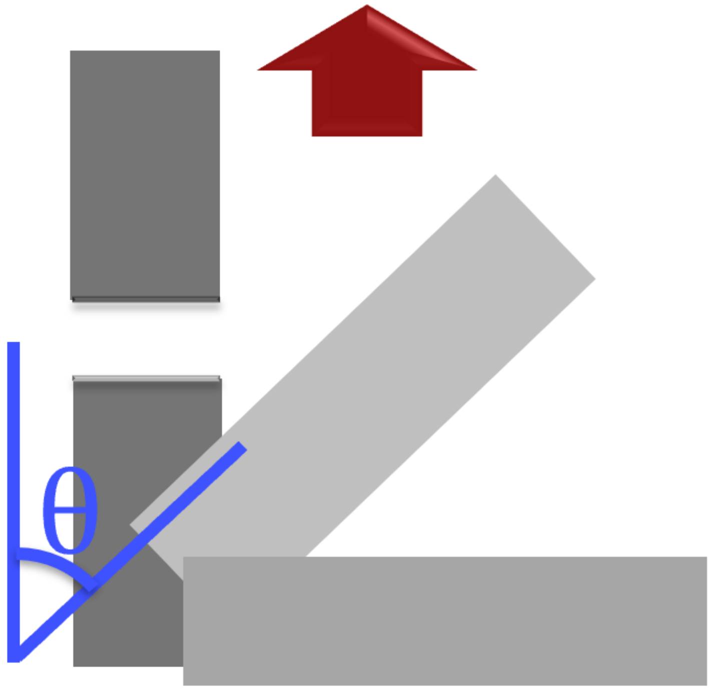

Mechanical analysis methods for ultra-stiff CFRP from thin tapes

A Master's thesis in Applied Mechanics by

MATTIAS PERSSON

Department of Industrial and Materials Science
Chalmers University of Technology
Gothenburg, Sweden 2019

Master's thesis 2019

Mechanical analysis methods for ultra-stiff CFRP from thin tapes

Master's thesis in Applied Mechanics

MATTIAS PERSSON

CHALMERS
UNIVERSITY OF TECHNOLOGY

Department of Industrial and Materials Science
Industrial and Materials Science
Chalmers University of Technology
Gothenburg, Sweden 2019

Mechanical analysis methods for ultra-stiff CFRP from thin tapes
Master's thesis in Applied Mechanics
MATTIAS PERSSON

Supervisor and examiner: Leif Asp, Professor at the Department of Industrial and Materials Science

Master's Thesis 2019
Department of Industrial and Materials Science
Division of Material and Computational Mechanics
Chalmers University of Technology
SE-412 96 Gothenburg
Telephone +46 31 772 1000

Cover: The failure mode of longitudinal tape fracture.

Typeset in LaTeX
Gothenburg, Sweden 2019

Mechanical analysis methods for ultra-stiff CFRP from thin tapes
Master's thesis in Applied Mechanics
MATTIAS PERSSON
Department of Industrial and Materials Science
Division of Material and Computational Mechanics
Chalmers University of Technology

Abstract

Today there is an increasing demand for more environmentally friendly transport systems. One way to decrease the fuel consumption of vehicles such as cars or airplanes is to decrease their weight. By replacing heavy construction material such as steel, which is often used in for example cars, with a material that has just as good mechanical properties as steel but a fraction of the weight, more fuel efficient vehicles could be made.

A carbon fibre composite material, constructed out of uniformly distributed ultra-thin high modulus carbon fibre reinforced polymer tapes, with mechanical properties approaching those of steel but with about a fifth of the density is the subject of study for this Master's thesis. The focus of the study was to construct mechanical analysis methods, i.e. models for predicting the stiffness and the strength in tensile loading, for the composite material that was manufactured and tested in an accompanying study with this thesis work.

The model was constructed in the numerical computation environment `MATLAB` and shows good agreement with the experimental results obtained from the tensile tests. The model predicts the stiffness, strength and failure modes most likely to occur in the laminate when loaded in tension. The model takes in-situ effects into account.

The first test and analysis results indicate great potential for the composite material as it exhibits tremendous mechanical properties even before the manufacturing has been perfected. The model also indicate failure of the laminate to initiate by tape pull-out followed by longitudinal tape fracture, and that transverse tape fracture is unlikely to occur for the simulated laminates.

Keywords: mechanical properties, composite, ultra-thin high modulus CFRP, mechanical analysis method, stiffness, strength, in-situ, tensile loading, tape pull-out, tape fracture.

Acknowledgements

First of all, I cannot stress enough how grateful I am for the support and guidance I have received from my supervisor Leif Asp, Professor at the department of Industrial and Materials Science. Without his inspiration and experience this project would not have been possible.

I would also like to thank Andreas Martsman, Fredrik Ohlsson and Florence Rinn at Oxeon, Professor Dan Zerkert at KTH, Fredrik Edgren at Volvo Cars and Spyros Tsampas and Adeline Kullerstedt at GKN Aerospace. They have all had an important role in everything from manufacturing and mechanical testing to contributing with their knowledge and experience.

I am also grateful to Brina Blinzler and David Carlstedt at Chalmers for their support and guidance. They have exhibited great patience in discussing various topics throughout this project.

And last but not least, I would like to thank the Swedish Innovation Agency VINNOVA for funding the project ”Stiff-tape” (2018-02856). Without financial support this project would not have been possible.

Mattias Persson, Gothenburg, June 2019

Contents

List of Figures

List of Tables

1
Introduction

This chapter gives an introduction to the Master's Thesis project including its purpose, limitations and a background to why it came to be.

1.1 Background

It is not uncommon that inspiration for new materials or products is found in nature. Such was the case when the idea for the material that is studied in this report was sprung. More specifically, the inspiration was found in nacre, the mother of pearls. Nacre is made up of staggered stiff inclusions embedded in a soft matrix. The stiff inclusions provides stiffness and carries load, while the soft matrix provides slip-planes in the material and transfers load via shear. This gives nacre tremendous stiffness, strength and damage tolerance [1],[2].

With an increasing demand for more environmentally friendly cars, airplanes and other ways of travel, there is an increasing demand for weight saving materials in industry. If one could replace the steel, that is often used as a construction material in for example cars, with a material that has just as good mechanical properties as steel but a fraction of the weight, more fuel efficient vehicles could be made.

In previous studies it has been shown that composite materials made with a high volume fraction of stiff inclusions that have a large length to thickness aspect ratio can have very impressive mechanical properties [3]. Because the ultra-thin carbon fibre composite tapes are as thin as 20 µm, even if a tape lay on top of another, the out-of-plane angle is extremely small. This means that a composite material made with these ultra-thin tapes can be modelled as a 2D-material, with all tapes ordered in the plane. Furthermore, if the tape orientations are uniformly distributed in-plane the composite has been shown to exhibit isotropic properties and can be modelled as a quasi-isotropic laminate using *The Equivalent Laminate Theory* (ELT) [4]. Traditional quasi-isotropic composite laminates with an equivalent eight ply lay-up of $[45°/-45°/0°/90°]_s$ have a minimum thickness of about 1000 µm. With the Ultra-Thin High Modulus Carbon Fibre Reinforced Polymer Tapes (UTHMT) of just 20 µm it is possible to manufacture an eight ply isotropic composite with a thickness of only 160 µm. This opens the possibility for design of much lighter structures than is possible today, and also for replacing sheet metals in for example cars.

Thus, with nacre as inspiration, a carbon fibre composite material with mechanical properties approaching those of steel but with about a fifth of the density (in theory) is manufactured and tested in affiliation with this thesis work. The composite is manufactured by another master's student, Marcus Johansen, who is doing his master's thesis in the same project as this thesis, the Stiff-Tape project, funded by VINNOVA, dnr. 2018-02856 [5]. The manufacturing was performed at Oxeon AB and the laminate was sent to KTH Royal Institute of Technology, where it was tested. Mr Johansen made the composite with UTHMT which are uniformly distributed in-plane. Both master's theses are part of a collaboration project between Chalmers University of Technology, Oxeon AB, KTH Royal Institute of Technology, Volvo Cars and GKN. The focus of Mr Johansen's thesis is the manufacturing, experimental tests and examination of the tested specimen, while the focus of this thesis is construction of computational models that can accurately predict the mechanical behaviour of this UTHMT composite laminate when it is loaded in tension. More specifically, computational models for the stiffness and the tensile strength of the composite.

1.2 Purpose

The aim of this project is to produce an engineering model that can accurately predict the elastic properties and strength of the UTHMT composite laminate that is to be manufactured. This model should be relatively easy to implement and adapt for different materials and dimensions of carbon fibre tapes. The model is to be constructed in the numerical computation environment `MATLAB` which will result in a model without demand for powerful computers. The out-put from the model should be easy to understand and should be limited to only information of relevance.

1.3 Boundaries

The boundaries of this project are determined by time. Within the scope of this project it is not realistic to aim for a complete model for all loading conditions, i.e., in-plane compression and shear loads. To achieve high-quality work, the focus for the stiffness and strength prediction is limited to loading in tension. This will ensure that enough laminates can be manufactured and tested to obtain reliable experimental results for verification of the model.

2
Literature study

This chapter contains information of relevance to the model construction, gathered in a literature study during the first few weeks of the project.

2.1 Stiffness prediction

Earlier studies of composites from discontinuous carbon fibre reinforced polymer (CFRP) tapes have been made by Takahashi and colleagues at University of Tokyo and by Pimenta and Robinson at Imperial College London. Takahashi determined the *Mori-Tanaka model* to be an accurate model for prediction of the tensile stiffness of discontinuous tape-based carbon fibre reinforced thermoplastics (CFRTP). The Mori-Tanaka model is of particular interest to the current work as it was demonstrated to accurately predict the elastic properties of CFRTP from uniformly distributed thin tapes [3]. The model is complicated and difficult to use in engineering models.

Pimenta and co-workers suggested to use an equivalent laminate model, considering the uniformly distributed tape composites as a quasi-isotropic lay-up of layers from UD discontinuous tapes, as illustrated in Figure 2.1.

Figure 2.1: Modeling of uniformly distributed UTHMT composite as an equivalent laminate, from [4].

ELT has been proven to provide accurate prediction of stiffness for discontinuous carbon fibre laminates with a quasi-isotropic lay-up [6].

In conference papers from 2016 and 2017 Takahashi and Wan presented results from their studies regarding the correlation between predictions with the Mori-Tanaka model and ELT of stiffness of composites of uniformly oriented discontinuous CFRP.

Data from experimental tensile tests were compared to data calculated with the two models, and the Mori-Tanaka model was found to accurately predict the stiffness while ELT was shown to over-estimate it slightly [7],[8].

Pimenta et al. [4] investigated the assumption that it was possible to model the random architecture of tow-based discontinuous composites (TBDCs) with high fibre-content using ELT and validate it experimentally. The investigation involved the manufacturing and testing of both TBDCs using randomly oriented tows as well as equivalent laminates. As Takahashi did earlier, they confirmed the assumption that the modeling strategy of using ELT is possible. Also, the influence of tow thickness was investigated and resulted in less stiff structures for increased tow thickness.

2.2 Strength prediction

Pimenta and Robinson [9] presented a fracture mechanics controlled strength model based on the mode II fracture toughness $\mathcal{G}_{IIC}$ at the interface between tapes, or *platelets*. The modeling approach taken by Pimenta and Robinson is complicated and would not fit the aim for an engineering model that is relatively easy to implement, but the fracture criterion for tape pull-out is of interest for the analytical model.

Li and Pimenta [10] presented a study of a multi-scale strength model which consists of a micro-scale stochastic shear-lag model, a meso-scale interactive-tension-shear criterion and a macro-scale ply discount method. In the study the model was shown to accurately predict the strength of quasi-isotropic equivalent laminates (QIELs) of discontinuous tows, while it over-estimates the strength of QIELs of corresponding randomly oriented TBDCs. The model considers the interaction between longitudinal and transverse stress components and is able to capture the failure mechanisms tow-failure and tow-debonding. In the study the failure envelopes of fracture criteria LaRC05, ITS and Tsai-Wu are compared. It is shown that the Tsai-Wu criterion yields a much smaller failure envelope than the other two since it does not take in-situ effects into account. It is also shown that LaRC05 slightly over-estimates the uni-axial tensile strength of TBDSs since it does not consider the interaction between longitudinal tension and transverse shear stresses. The small difference between the results of ITS and LaRC05 is contributed to the fact that the tension-shear interaction is small in a TBDCs under uni-axial loading, where the failure of the most critical plies is dominated by longitudinal stress . Another failure criterion that is of interest for this project is the set of criteria by Hashin failure criteria for unidirectional fibre composites [11]. These criteria take both tensile and shear stress into account.

Camanho et al. [12] presented a study regarding prediction of matrix cracking and in-situ strengths in composites and accounts for transverse tension and in-plane shear. The transverse tensile and shear strengths of a ply in unidirectional laminate is lower than for a ply that is constrained by plies with different fibre orientations and thus experience in-situ effects. The Hashin failure criteria do not account for the in-situ effects, which is an important part in strength prediction for plies with uniformly distributed tapes. The Hashin criteria would thus need to be supplemented with an in-situ effect if the model is to be accurate.

In an article addressing simulation of the mechanical response of thin-ply composites, Arteiro et al. [13] plot predictions of how the in-situ transverse tensile strength increases with decreasing ply thickness. Their predictions, shown in Figure 2.2 demonstrates the importance of in-situ effects for thin-ply composites like those studied in the current investigation.

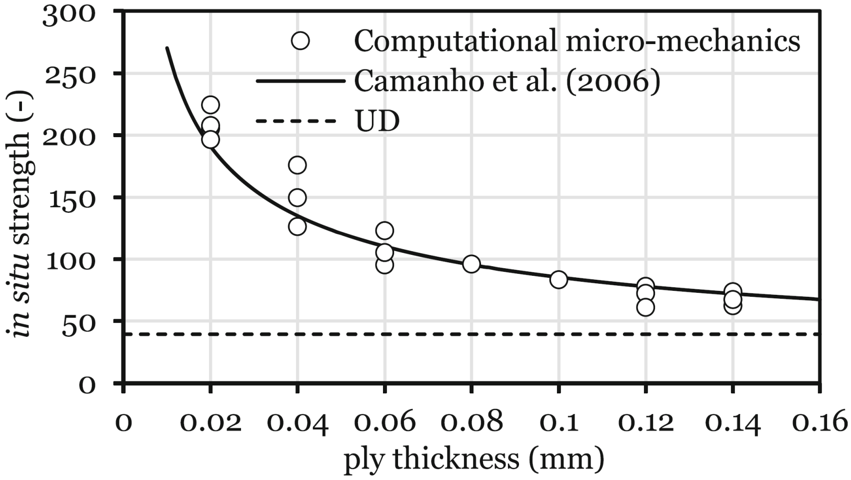

Figure 2.2: In-situ transverse tensile strength as a function of ply thickness, from [13].

3

Theory

In this section the theory behind the analytical models is presented. The theory is gathered from books and scientific articles.

3.1 Material properties and volume fractions

Different types of carbon fibres have different mechanical properties such as strength, stiffness E_f, Poisson's ratio ν_f, fibre strain to fracture X_f and density ρ_f. Thus variables for the *fibres* will be denoted with the subscript f. Mechanical properties for the resin, or *matrix*, are denoted with the subscript m. When calculating the stiffness of the laminate in section 3.2 the volume fractions of fibres and matrix are needed. This is not always a known value for the manufacturer of the laminate since it is easier to calculate the weight percentage of fibres and matrix, w_f and w_m. The way to calculate the volume fractions when only the weight percentage is known is by a calculation of the weight fractions W_f and W_m as $w_f/100$ and $w_m = 1 - w_f$ and then the volume fractions as

$$V_f = \frac{W_f}{W_f + W_m \frac{\rho_f}{\rho_m}}, \qquad V_m = 1 - V_f \tag{3.1}$$

3.2 Elastic properties

To calculate the stiffness of the laminate the elastic properties, i.e., the stiffness E and the shear moduli G in both the longitudinal and the transverse direction, are first calculated for each individual ply. The global stiffness of the composite E_c can then be calculated as well as the stiffness depending on the angle of tapes $E_{tape}(\theta)$ which is needed in the strength prediction where the first tape failure is the limiting factor.

3.2.1 CLT to ELT

The theory for calculations of mechanical properties of individual composite plies placed on top of each other to construct a composite laminate is called Classical Laminate Theory (CLT). Depending on the fibre arrangement of the individual plies the laminate can exhibit different characteristics, see Figure 3.1. For example, if the plies are not placed balanced and symmetrically on both sides of a mid-plane, see Figure 3.2, the laminate will warp when loaded. If a discontinuous fibre composite is constructed in such a way that it is exhibiting isotropic properties in the xy-plane it can be addressed using laminate theory. However, since it lacks the order that follows for a stacked continuous fibre composite (rather having fibre tapes with random orientations in the "same plane") the laminate properties are calculated from it's equivalent continuous fibre laminate lay-up. We call this Equivalent Laminate Theory (ELT). For a fully uniform distribution of tape orientations the calculation shows the laminate to be isotropic.

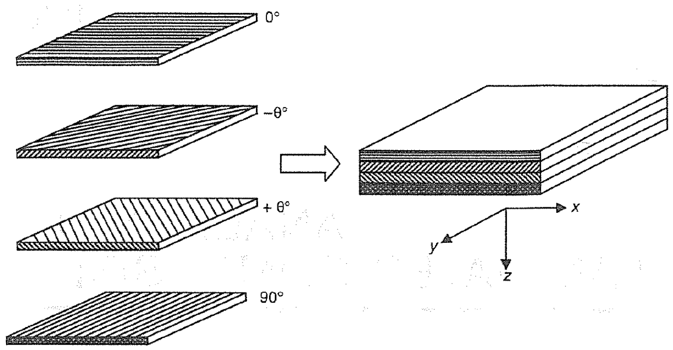

Figure 3.1: Fibre directions of individual plies, from [6].

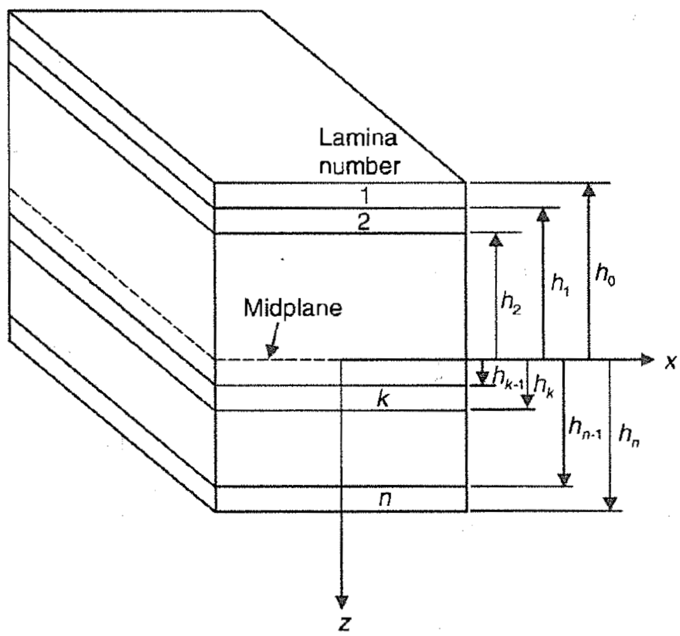

Figure 3.2: Mid-plane explanation, from [6].

The assumption that we can indeed achieve an isotropic material is the starting point of the calculation of the mechanical properties for the UTHMT composite studied here. According to ELT a laminate consisting of plies with continuous fibres and the lay-up $[45°/-45°/90°/0°]_s$ will result in a quasi-isotropic laminate. Thus a model that uses eight plies of continuous directional fibres should result in a quasi-isotropic laminate model that accurately predicts the stiffness of the UTHMT.

In laminate theory it is assumed that the out-of-plane shear strains γ_{xz} and γ_{yz} are zero. This assumption is based on the assumption that a section of a laminate that is originally perpendicular to the laminate mid-plane remains perpendicular to the mid-plane if the laminate is deformed. [6]

3.2.2 Elastic properties of individual lamina

The Longitudinal stiffness of a lamina, i.e. a ply, is calculated with the rule of mixtures,

$$E_L = V_f E_f + V_m E_m \tag{3.2}$$

where the subscripts f and m stands for *fibres* and *matrix* respectively. The transverse stiffness however is calculated with the Halpin-Tsai model for transverse stiffness prediction. This is because in reality the stresses in the matrix and the fibres are not equal. Thus the transverse stiffness is calculated as

$$E_T = E_m \frac{1 + \xi \eta V_f}{1 - \eta V_m},\ \eta = \frac{(0.05 \cdot E_f / E_m) - 1}{(0.05 \cdot E_f / E_m) + \xi} \tag{3.3}$$

where the curve fitting parameter $\xi = 2$ for circular fibres. Also, since the fibres are not isotropic η is approximated using the transverse fibre stiffness as 5% of the longitudinal fibre stiffness.

The major Poisson's ratio ν_{LT}, minor Poisson's ratio ν_{TL} and the shear modulus G_{LT} are calculated as

$$\nu_{LT} = \nu_f V_f + \nu_m V_m \tag{3.4}$$

$$\nu_{TL} = \nu_{LT} \frac{E_T}{E_L} \tag{3.5}$$

$$G_{LT} = G_m \frac{1 + \xi_G \eta_G V_f}{1 - \eta_G V_f} \tag{3.6}$$

with $\xi_G = 1$ and η_G being the Halpin-Tsai curve fitted parameters for the shear modulus. η_G is calculated with the same assumption of the transverse fibre stiffness as in Equation 3.3 for the fibre shear modulus, and with the matrix shear modulus

$$G_f = \frac{(0.05 \cdot E_f) - 1}{2(1 + \nu_f)} \tag{3.7}$$

$$G_m = \frac{G_m}{2(1 + \nu_m)} \tag{3.8}$$

$$\eta_G = \frac{(G_f / G_m) - 1}{(G_f / G_m) + \xi_G} \tag{3.9}$$

To calculate the elastic properties of the laminate the stiffness matrix Q is needed. With the elastic properties of each individual lamina Q is calculated as

$$[\boldsymbol{Q}] = \begin{bmatrix} \dfrac{E_L}{1-\nu_{LT}\nu_{TL}} & \dfrac{\nu_{LT}E_L}{1-\nu_{LT}\nu_{LT}} & 0 \\ \dfrac{\nu_{LT}E_T}{1-\nu_{LT}\nu_{LT}} & \dfrac{E_T}{1-\nu_{LT}\nu_{LT}} & 0 \\ 0 & 0 & G_{LT} \end{bmatrix} \tag{3.10}$$

The transformation matrices $[\boldsymbol{T}_1]$ and $[\boldsymbol{T}_2]$ are then used to transform the directional properties of each individual laminae to the global coordinates of the laminate as

$$[\bar{\boldsymbol{Q}}] = [\boldsymbol{T}_1]^{-1}[\boldsymbol{Q}][\boldsymbol{T}_2] \tag{3.11}$$

$[\boldsymbol{T}_1]$ and $[\boldsymbol{T}_2]$ are defined as

$$[\boldsymbol{T}_1] = \begin{bmatrix} \cos^2\varphi & \sin^2\varphi & 2\sin\varphi\cos\varphi \\ \sin^2\varphi & \cos^2\varphi & -2\sin\varphi\cos\varphi \\ -\sin\varphi\cos\varphi & \sin\varphi\cos\varphi & \sin^2\varphi-\cos^2\varphi \end{bmatrix} \tag{3.12}$$

$$[\boldsymbol{T}_2] = \begin{bmatrix} \cos\varphi^2 & \sin^2\varphi & \sin\varphi\cos\varphi \\ \sin^2\varphi & \cos^2\varphi & -\sin\varphi\cos\varphi \\ -2\sin\varphi\cos\varphi & 2\sin\varphi\cos\varphi & \cos^2\varphi-\sin^2\varphi \end{bmatrix} \tag{3.13}$$

with φ being the angle of the individual laminae. With this the extensional stiffness matrix of the laminate constructed of k number of individual lamina can be calculated as a summation of the $[\bar{\boldsymbol{Q}}]_k$ matrices and the corresponding thickness $(h_k - h_{k-1})$ of the k plies.

$$\boldsymbol{A}_{ij} = \sum_{k=1}^{n}[\bar{\boldsymbol{Q}}_{ij}]_k(h_k - h_{k-1}) \tag{3.14}$$

The matrix $[\bar{\boldsymbol{a}}]$ which contains the in-plane effective moduli can now be defined [14]., given the assumption that the lay-up is symmetric, as

$$[\bar{\boldsymbol{a}}] = t_{tapes}[\boldsymbol{A}]^{-1} \tag{3.15}$$

The effective in-plane moduli, with respect to the global coordinates of the laminate and $E_{tape}(\theta)$ depending on the angle of the tapes, can thus be estimated as

$$E_c = 1/\bar{\boldsymbol{a}}_{11} \tag{3.16}$$

and

$$E_{tape}(\theta) = \frac{1}{\dfrac{\cos^4(\theta)}{E_L} + \dfrac{\sin^4(\theta)}{E_T} + \dfrac{\sin^2(2\theta)}{4}\left(\dfrac{1}{G_{LT}} - 2\dfrac{\nu_{LT}}{E_L}\right)}, \quad 0° \leq \theta < 90° \tag{3.17}$$

3.3 Strength prediction

3.3.1 Failure modes

There are two ways in which the laminate can fail: tape pull-out, see Figure 3.3(b), or tape fracture, see Figures 3.3(c)-3.3(d). Thus, to predict the strength of the laminate the critical mode that initiates failure of the laminate needs to be identified. This is because the first failure is the limiting factor of the strength of the laminate.

Since the distribution of tapes are uniform there will be tapes oriented at all angles $0° \leq \theta < 90°$ with respect to the direction of the load. The critical failure mode will be different for different angles of tapes, which means that there may be a transition from one failure mode to another somewhere between $0° \leq \theta < 90°$, or at several angles. Tapes of different constituents will of course yield different properties for the laminate and thus move the point (or points) of transition between the failure modes.

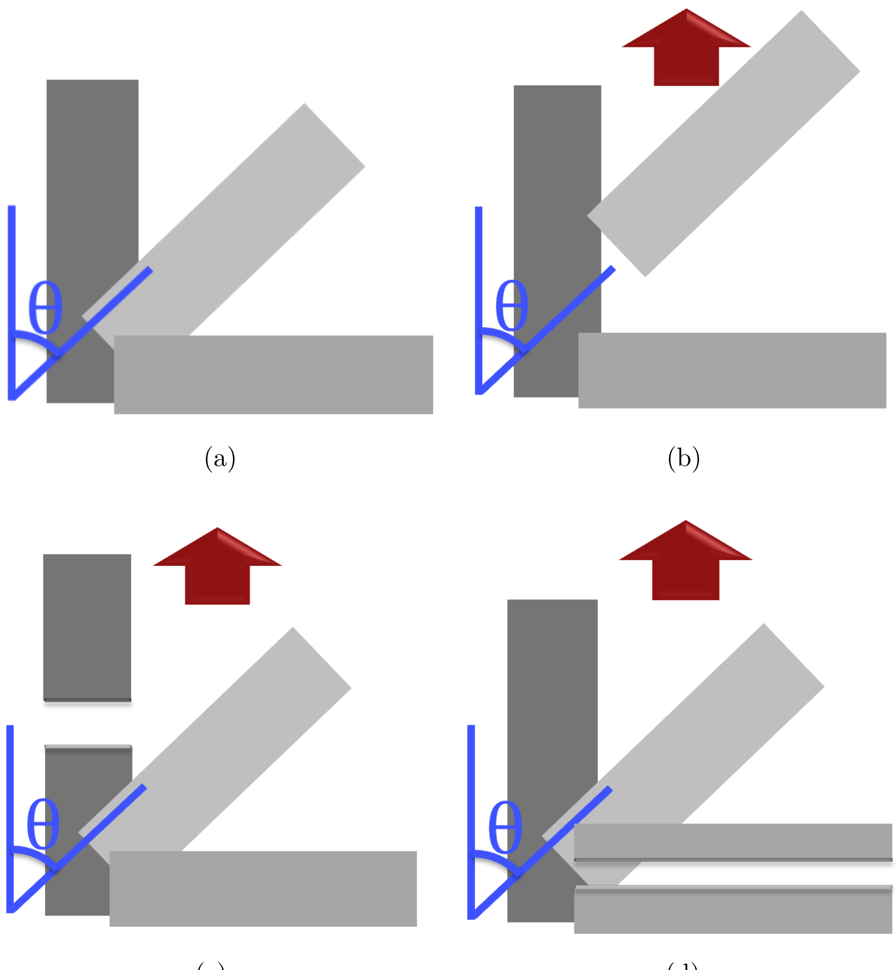

(a) (b) (c) (d)

Figure 3.3: Different fracture modes: (a) pristine laminate; (b) pull-out; (c) longitudinal fracture; and, (d) transverse fracture.

3.3.2 Loading condition

In most applications, composite laminates are loaded in the plane, which produces a condition of plane-strain, which means that the out-of-plane stress components are zero. If the out-of-plane axis is axis 3, then the plane-stress condition yields $\sigma_3 = \tau_{13} = \tau_{23} = 0$. This also means that the shear strain $\gamma_{13} = \gamma_{23} = 0$.

Laminates are manufactured in a way that it can be assumed that the bonds between the plates are infinitesimally thin and do not deform in shear, so the plates cannot slip over each other. Laminates can thus be assumed to act as single-layer materials, and displacements remain continuous across an intersection perpendicular to the laminates mid-plane. Stress can vary across the intersection, but the strain is the same if there is no debonding. Therefore the strength prediction for the laminate will be strain-based instead of stress based.

3.3.3 Tape pull-out

As mentioned in section 2 Pimenta and Robinson presented a fracture mechanics controlled strength model based on the mode II fracture toughness $\mathcal{G}_{IIC}$ in the interface between tapes. A strain-based expression of this model is

$$\varepsilon_{pull-out} = \frac{1}{E_c}\sqrt{\frac{2E_{tape}(\theta)\mathcal{G}_{IIC}}{\pi t_{tape}}} \tag{3.18}$$

where t_{tape} is the tape thickness, E_c is the stiffness of the composite and $E_{tape}(\theta)$ is the stiffness of the tapes depending on their angle with respect to the load.

3.3.4 Tape fracture

Camanho et al. gives the equation for in-situ transverse tensile strength for a thin embedded ply in pure mode I loading [12]. With this, the in-situ transverse tensile strain to failure can be determined as

$$\varepsilon^T_{Y,is} = \frac{1}{E_{tape}(\theta)}\sqrt{\frac{8\mathcal{G}_{IC}}{\pi t \Lambda^o_{22}}} \quad \text{with} \tag{3.19}$$

$$\Lambda^o_{22} = 2\left(\frac{1}{E_2} - \frac{\nu^2_{21}}{E_1}\right) \tag{3.20}$$

Where ν_{21} is ν_{LT} calculated using ELT. Camanho also states the expressions for in-situ shear strength of thin embedded plies as well as thin outer plies. For a more conservative strength prediction the expression for thin outer plies is used in the model. Also this expression is converted to achieve the in-situ shear strain to failure as

$$\varepsilon^T_{S,is} = \frac{2}{G_{LT}}\sqrt{\frac{G_{LT}\mathcal{G}_{IIC}}{\pi t_{tape}}} \tag{3.21}$$

It should be noted that this is the expression for the linear case and not the non-linear case, which is also provided in the paper by Camanho and co-workers. The linear case is more conservative than the non-linear case, and can be demonstrated by a plot of the linear and non-linear strength prediction of the in-situ shear strength of a thin surface ply, given by Camanho et al. depicted in Figure 3.4.

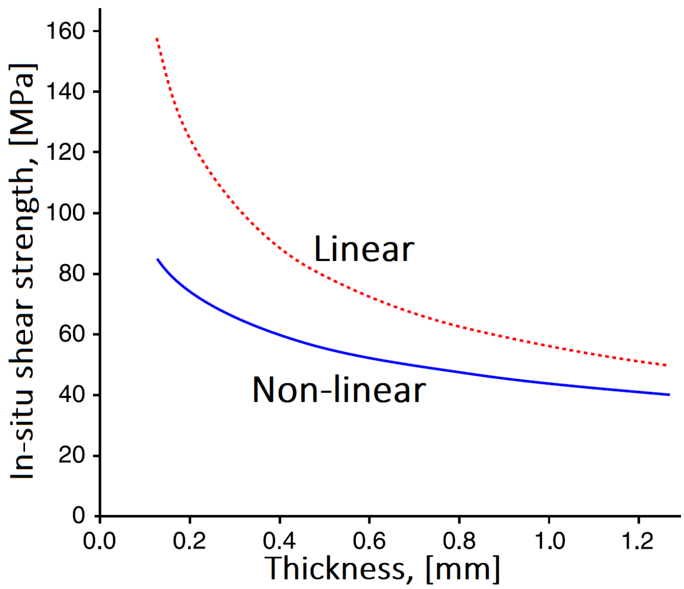

Figure 3.4: Linear and non-linear case of in-situ shear strength as function of thickness, from Camanho et al. [12].

The fracture criteria for tape fracture that are used in this model are the Hashin failure criteria. Strain-based expressions of the Hashin criteria for fibre dominated fracture ε_1^D, and matrix dominated fracture ε_2^D, is given by Adoubi et al [15].

$$\varepsilon_1^D = \sqrt{\left(\frac{\varepsilon_{11}}{X_e}\right)^2 + \left(\frac{\gamma_{12}}{\varepsilon_{S,is}^T}\right)^2} \tag{3.22}$$

$$\varepsilon_2^D = \sqrt{\left(\frac{\varepsilon_{22}}{\varepsilon_{Y,is}^T}\right)^2 + \left(\frac{\gamma_{12}}{\varepsilon_{S,is}^T}\right)^2} \tag{3.23}$$

where ε_{11}, ε_{22}, are the normal engineering in-plane strains, γ_{12} is the engineering shear strain and X_e is the longitudinal strain to failure of the fibres. By using the transformation matrix $[\boldsymbol{T}_2]$ for the strain components, given the isotropic properties, gives the fibre and the matrix dominated expressions as

$$\begin{Bmatrix} \varepsilon_{11} \\ \varepsilon_{22} \\ \gamma_{12} \end{Bmatrix} = [\boldsymbol{T}_2] \begin{Bmatrix} \varepsilon \\ 0 \\ 0 \end{Bmatrix} \tag{3.24}$$

$$\varepsilon_1^D = \varepsilon \sqrt{\frac{\cos^4(\theta)}{X_e^2} + \frac{4\sin^2(\theta)\cos^2(\theta)}{(\varepsilon_{S,is}^T)^2}} \tag{3.25}$$

$$\varepsilon_2^D = \varepsilon \sqrt{\frac{\sin^4(\theta)}{(\varepsilon_{Y,is}^T)^2} + \frac{4\sin^2(\theta)\cos^2(\theta)}{(\varepsilon_{S,is}^T)^2}} \tag{3.26}$$

Damage initiation is predicted to initiate when $\varepsilon_1^D = 1$ or $\varepsilon_2^D = 1$. The longitudinal and the transverse strain with Hashin failure criteria can thus be expressed as

$$\varepsilon_{tape,L} = \frac{1}{\sqrt{\frac{\cos^4(\theta)}{X_e^2} + \frac{4\sin^2(\theta)\cos^2(\theta)}{(\varepsilon_{S,is}^T)^2}}} \tag{3.27}$$

$$\varepsilon_{tape,H} = \frac{1}{\sqrt{\frac{\sin^4(\theta)}{(\varepsilon_{Y,is}^T)^2} + \frac{4\sin^2(\theta)\cos^2(\theta)}{(\varepsilon_{S,is}^T)^2}}} \tag{3.28}$$

3.3.5 Damage initiation

The lowest computed value for strain to failure of three possible failure modes is identified to initiate failure in the composite. Pull-out is given by Equation (3.18), longitudinal tape fracture by Equation (3.27) and transverse tape fracture by Equation (3.28) for all angles $0° \leq \theta < 90°$ can now be determined. The smallest of all these strains is the laminate damage initiation strain, $\hat{\varepsilon}_\theta$, determining the strength of the laminate.

4

Results

In this section the results from the analytical model made with use of the theory in the Theory section are presented. Also presented are the results from the experimental tensile tests, as well as a comparison between the analytical and the experimental results.

4.1 Material data and conditions for comparison

The dimensions of the carbon fibre tapes for which the laminate properties are calculated are $40 \times 20 \times 0.0225$ [mm] ($l \times w \times t$). In the beginning the thickness of the tapes was 20μm but due to difficulties to achieve quality laminates in the manufacturing the tapes had to be provided with a layer resin on the side which previously had none. This also led to a lower fibre volume fraction than targeted. The goal in the end is to reach a fibre volume fraction of approximately 60 %, but at this stage the most important thing is to produce high-quality laminates for reliable experimental test results. There were two laminates manufactured for the experimental tensile tests, one with $V_f = 44.1$ % and one with $V_f = 47.7$ %. The average volume fraction of these laminates $V_f = 45.9$ % is used for comparison with the analytical model, as well as the average stiffness and strength. Thus, the data for the carbon fibre tapes, the matrix and laminate properties are displayed in Tables 4.1-4.2 below.

Table 4.1: Material properties of the HS40 carbon fibre.

V_f	ρ_f $[g/cm^3]$	E_f [GPa]	ν_f	X_e [%]
0.459	1.82	425	0.2^a	1.1

[a]Assumed Poisson's ratio. Not stated in HS40 data sheet

Table 4.2: Material properties of the matrix used in the current study.

V_m	ρ_m $[g/cm^3]$	E_m [GPa]	ν_m	X_m[%]
0.541	1.15	3.5	0.33	2.2

4.2 Stiffness prediction

In using the analytical model with input as stated in Tables 4.1-4.2 and Equations (3.1)-(3.17) the stiffness of the laminate is estimated to $E_c = 70.6$ GPa. The calculated mechanical properties for the laminate pertinent to the strength prediction can be summarised in Tables 4.3 below.

Table 4.3: Estimated Properties of the laminate with HS40 carbon fibres (V_f = 45.9%) and matrix.

t_{tape} [μm]	E_c [GPa]	G_{LT} [GPa]	$\mathcal{G}_{IC}$ [J/m^3]	$\mathcal{G}_{IIC}$ [J/m^3]	Y_T [MPa]
22.5	70.6	2.67	230[a]	400[b]	50[c]

[a]Assumed value for mode I fracture toughness, from Asp et al. [16]
[b]Assumed value for mode II fracture toughness, from Asp et al. [16]
[c]Assumed transverse strength

4.3 Strength prediction and fracture modes

As mentioned in Section3.3 strength prediction considers two fracture modes, tape pull-out and tape fracture. The first mode to be evaluated is tape pull-out. By using Equations (3.17)-(3.18) with mechanical properties stated in Table 4.3 the strain at damage initiation via tape pull-out is estimated for all tape angles and saved as a vector $\varepsilon_{pull-out}$. This is visualised in Figure 4.1.

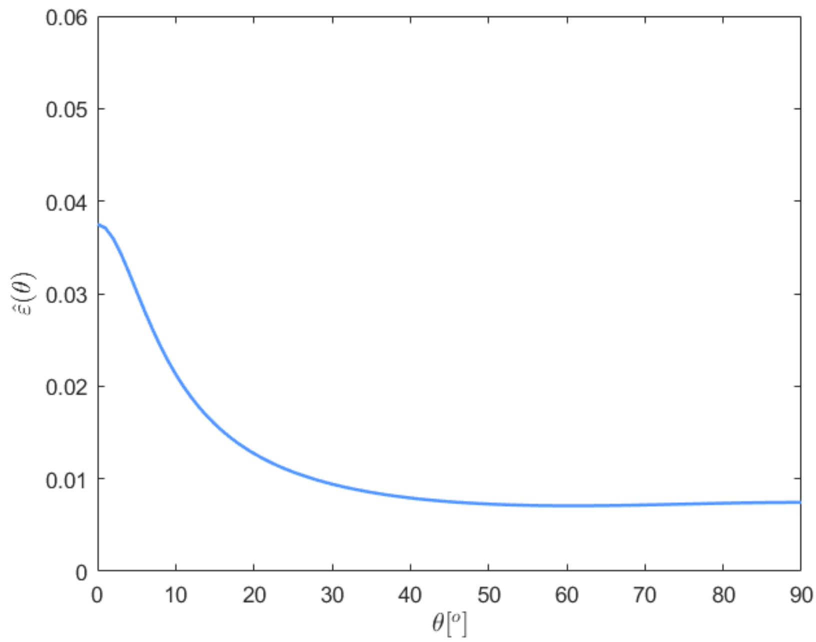

Figure 4.1: Damage initiation strain for tape pull-out with $t_{tape} = 22.5$ μm and $V_f = 45.9\%$.

The strain at damage initiation via longitudinal and transverse tape fracture are estimated as described in Section 3.3.4 and saved as vectors in the same way as for tape pull-out, $\varepsilon_{tape,L}$ and $\varepsilon_{tape,T}$, and visualised in Figures 4.2 and 4.3.

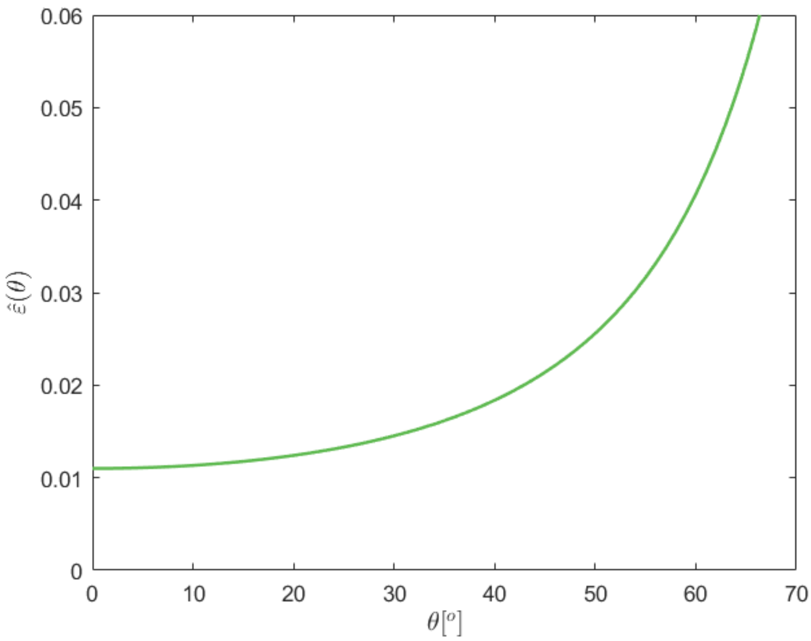

Figure 4.2: Damage initiation strain for longitudinal tape fracture with $t_{tape} = 22.5$ μm and $V_f = 45.9\%$.

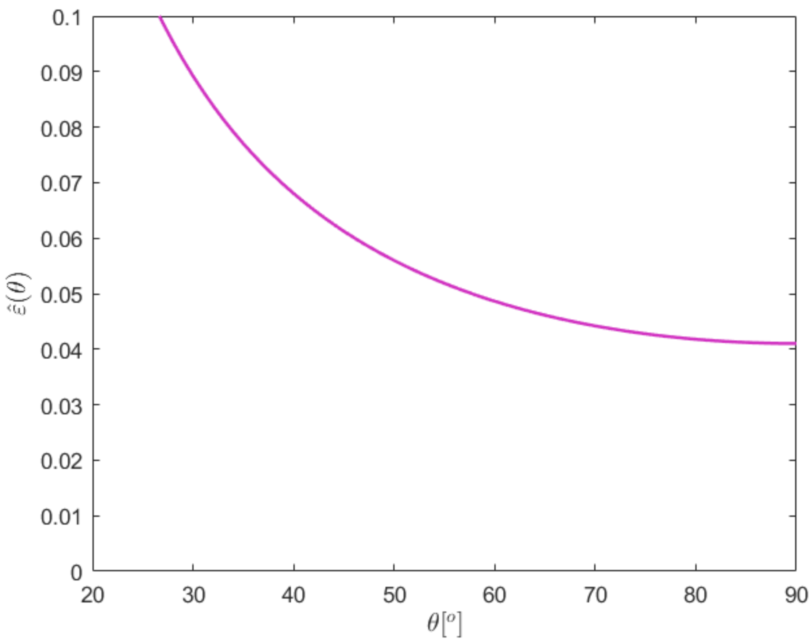

Figure 4.3: Damage initiation strain for transverse tape fracture with $t_{tape} = 22.5$ μm and $V_f = 45.9\%$.

By taking the minimum damage initiation strain for all three fracture modes at all tape angles a new vector can be defined as $\hat{\varepsilon}$. This is visualised as the full black line in Figure 4.4 which contains the damage initiation strain for all fracture modes as well as the minimum damage initiation strain, $\hat{\varepsilon}(\theta)$.

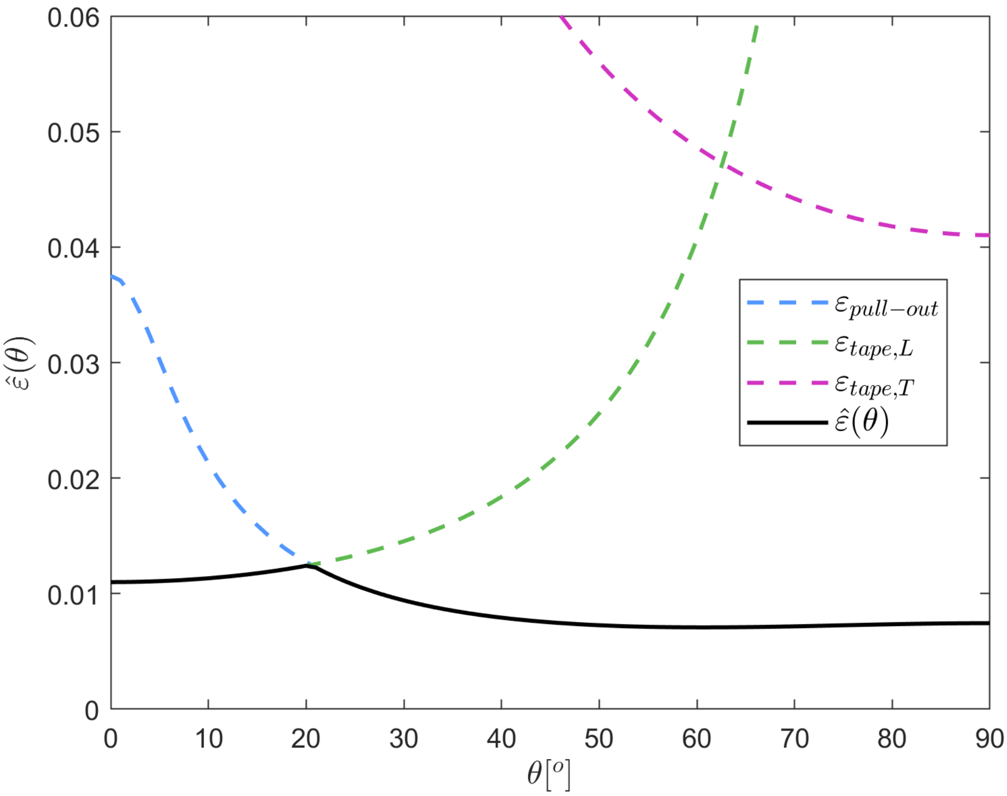

Figure 4.4: Damage initiation strain for all fracture modes with $t_{tape} = 22.5\ \mu$m and $V_f = 45.9\%$.

As can be seen in the Figure, the dominating fracture mode for tapes with angle $0 \leq \theta \lesssim 21°$ is the longitudinal tape fracture, and for $21° \lesssim \theta \leq 90°$ tape pull-put is the dominating mode. By taking the smallest value of $\hat{\varepsilon}$ the damage initiation strain and fracture mode for the laminate is predicted to be $\hat{\varepsilon} = 0.7\%$, with the fracture mode pull-out at approximately 62°. By using Hooke's Law the strength of the laminate $\hat{X}$ can be estimated as

$$\hat{X} = E_c \cdot \hat{\varepsilon} \approx 494.2 \text{ MPa} \tag{4.1}$$

4.4 Comparison with experimental results

A comparison of the results from the analytical model and the results obtained from the mechanical tensile tests, with the data as mentioned in Section 4.1 being the average data of the two tested laminates, are presented in Figure 4.5 below.

HS40	$V_f = 45.9$ %, $t = 22.5$ µm, $X_e = 1.1$ % $\mathcal{G}_{IIC} = 400$ J/m², $E_f = 425$ GPa	
	Predicted	Experimenal Results
E_c [GPa]	70.6	64.2 (±11.3)
$\hat{\varepsilon}$ [%]	0.70	0.59 (±0.11)
Mode	Pull-out	Pull-out/Tape Fracture
$\hat{X}$ [MPa]	494.2	395.3 (±77.6)

Figure 4.5: Comparison of analytical and experimental results of mechanical properties for the laminate with the standard deviation for the experimental results inside the parentheses (experimental data from [5]).

4.5 Simulation of three alternative carbon fibres

A laminate with $V_f = 59.19\%$ was targeted in the project. However, such a laminate could not be manufactured during the short time the project was run [5]. Instead, as mentioned in Section 4.1, two laminates with $V_f = 44.1\%$ and $V_f = 47.7\%$ was achieved, resulting in the average fibre volume fraction of $V_f = 45.9\%$ used in the previous analysis. However, by fine-tuning the manufacturing process we expect to be able to produce high-quality laminates with a fibre volume fraction approaching 60 % in the near future.

To see what mechanical properties that can be expected if the laminate was manufactured with a fibre volume fraction approaching 60% and another type of carbon fibre than HS40, a simulation of HS40 and three other common carbon fibres, T300, HM63 and K13916, was made with the fibre volume fraction of $V_f = 59.19\%$ and the same matrix used in the current study matrix. The analytical results of this simulation are presented in Figure 4.6.

	$V_f = 59.19$ %, $t = 22.5$ µm, $\mathcal{G}_{IIC} = 400$ J/m^2			
	T300	HS40	HM63	K13916
E_f [GPa]	230	425	441	760
X_e [%]	1.5	1.1	1	0.4
E_c [GPa]	50.51	90.48	93.43	159.92
$\hat{\varepsilon}$ [%]	0.96	0.62	0.60	0.38
Mode	Pull-out	Pull-out	Pull-out	Pull-out
$\hat{X}$ [MPa]	487	560	562	618

Figure 4.6: Comparison of analytical results for the carbon fibres T300, HS40, HM63 and K13916 with $V_f = 59.19\%$.

4.6 Simulation with higher volume fraction and fracture toughness

Another goal than higher fibre volume fraction is to achieve higher mode II fracture toughness than the assumed $\mathcal{G}_{IIC} = 400\,\mathrm{J/m^2}$ which was used in the previous simulations. The mode II fracture toughness could be improved, which is further explained in the Future work Section 5.3, and a feasible fracture toughness of $\mathcal{G}_{IIC} = 1100\,\mathrm{J/m^2}$ [16] is expected. Expected mechanical properties if these targets are reached are presented in Figure 4.7.

	$V_f = 59.19$ %, $t = 22.5$ µm, $\mathcal{G}_{IIC} = 1100$ J/m^2			
	T300	HS40	HM63	K13916
E_f [GPa]	230	425	441	760
X_e [%]	1.5	1.1	1	0.4
E_c [GPa]	50.51	90.48	93.43	159.92
$\hat{\varepsilon}$ [%]	1.5	1.03	1.0	0.4
Mode	Tape Fracture	Pull-out	Pull-out	Tape Fracture
$\hat{X}$ [MPa]	758	930	935	640

Figure 4.7: Comparison of mechanical properties for T300, HS40, HM63 and K13916 with $V_f = 59.19\%$ and $\mathcal{G}_{IIC} = 1100\,\mathrm{J/m^2}$.

4.7 Influence of different properties

It is of interest to know what influence different material properties have on the mechanical properties of the laminate. As can be seen in Equation 3.18 the damage initiation strain for tape pull-out is inversely proportional to the thickness of the tapes, t_{tape}. It can also be seen in Equations 3.19, 3.21 and 3.27-3.28 that the damage initiation strains for tape fracture are influenced by the tape thickness. Also in Equations 3.18 and 3.21 it can be seen that both tape pull-out and tape fracture are proportional to the mode II fracture toughness, $\mathcal{G}_{IIC}$. From Equations 3.18 and 3.19 it can be noted that the stiffness of the laminate influences the damage initiation strains. Therefore, a change of stiffness E_f is of interest since it has a direct influence on the stiffness of the laminate. However, with a change in fibre stiffness comes most likely a change in fibre strain to failure X_e, as can be seen in Figures 4.6 and 4.7. Thus, to obtain a realistic evaluation of the influence of fibre stiffness, the fibre strain to failure will have to change with the fibre stiffness. Therefore, a least square fit of E_f and X_e is performed.

4.7.1 Least square fit of E_f and X_e

The fibre stiffness E_f and fibre strain to failure X_e of the different types of carbon fibres that were used in the simulations in Sections 4.5 and 4.6 are used in the least square fit evaluation, to get an approximation of the change in X_e with E_f. The least square fit yields Equation (4.2), which is also demonstrated as the dotted line in Figure 4.8.

$$E_f = -4814.5 \cdot 10^{11} \cdot X_e + 9454.5 \cdot 10^8 \tag{4.2}$$

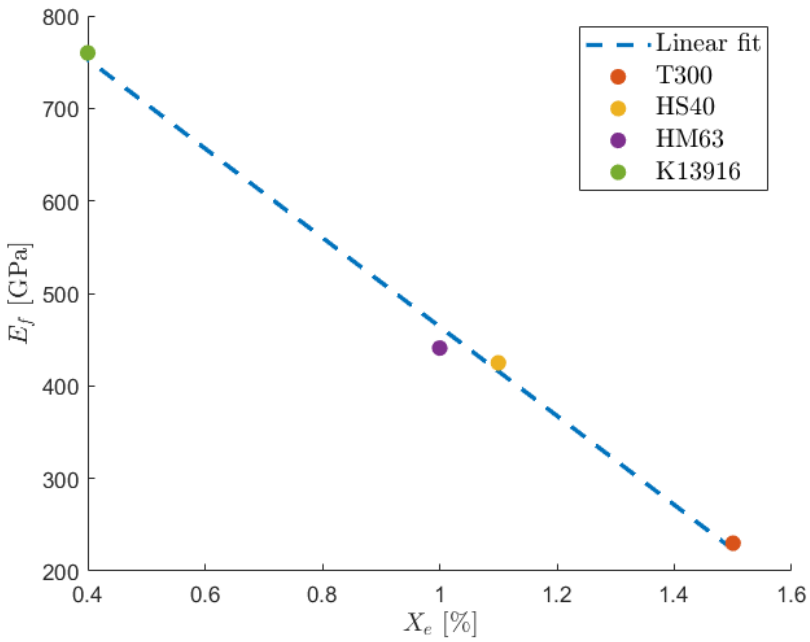

Figure 4.8: Least square fit of E_f vs. X_e for T300, HS40, HM63 and K13916.

4.7.2 Damage initiation strain depending on t_{tape}, $\mathcal{G}_{IIC}$, E_f

It is of interest to know how the mechanical properties of the laminate change when changing t_{tape}, $\mathcal{G}_{IIC}$ and E_f. By having the standard values and intervals for iteration seen in Table 4.4, changing one property at the time and keeping the other two constant, Figures 4.9-4.11 were made. For easier interpretation arrows have been drawn in the figures illustrating in which direction the damage initiating strain changes for the different fracture modes when increasing the specified property, with the smallest and largest value written adjacent $\varepsilon_{pull-out}$ and $\theta = 0$.

Table 4.4: Values for the iteration analysis.

	Standard value	Interval for iteration
t_{tape}	22.5 μm	$10 \leq t_{tape} \leq 185$ μm
$\mathcal{G}_{IIC}$	400 J/m^3	$100 \leq \mathcal{G}_{IIC} \leq 2000$ J/m^3
E_f	425 GPa	$200 \leq E_f \leq 800$ GPa

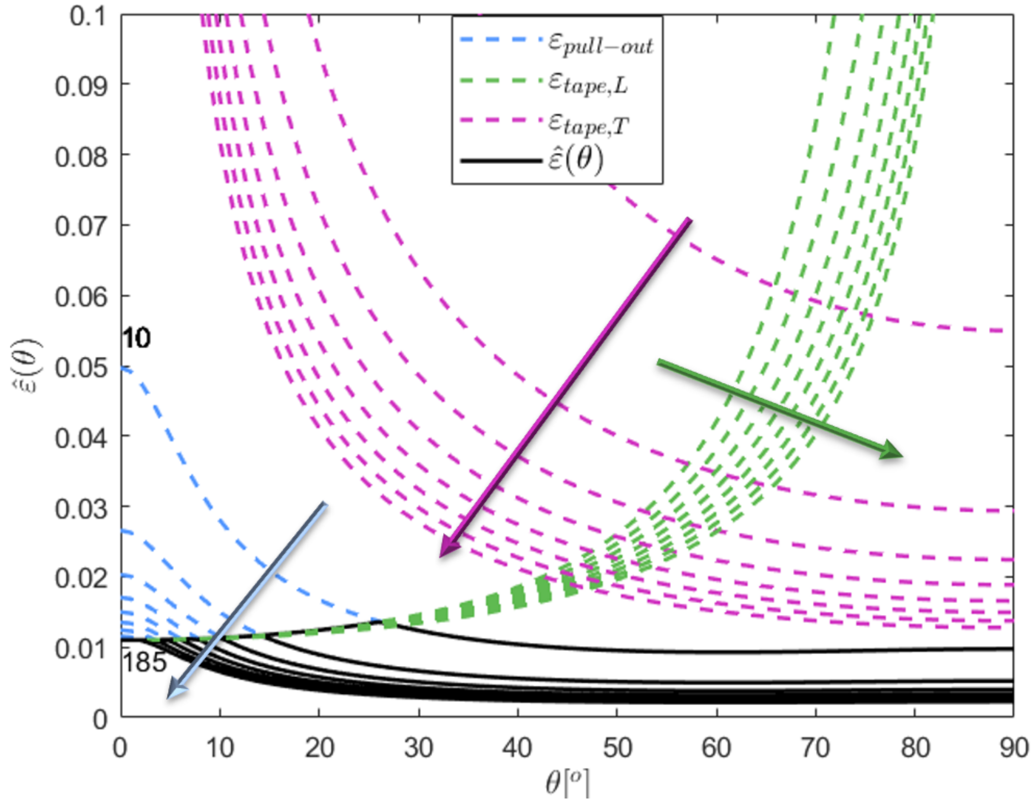

Figure 4.9: Damage initiation strains depending on t_{tape} with $E_f = 425$ GPa and $\mathcal{G}_{IIC} = 400$ J/m^3.

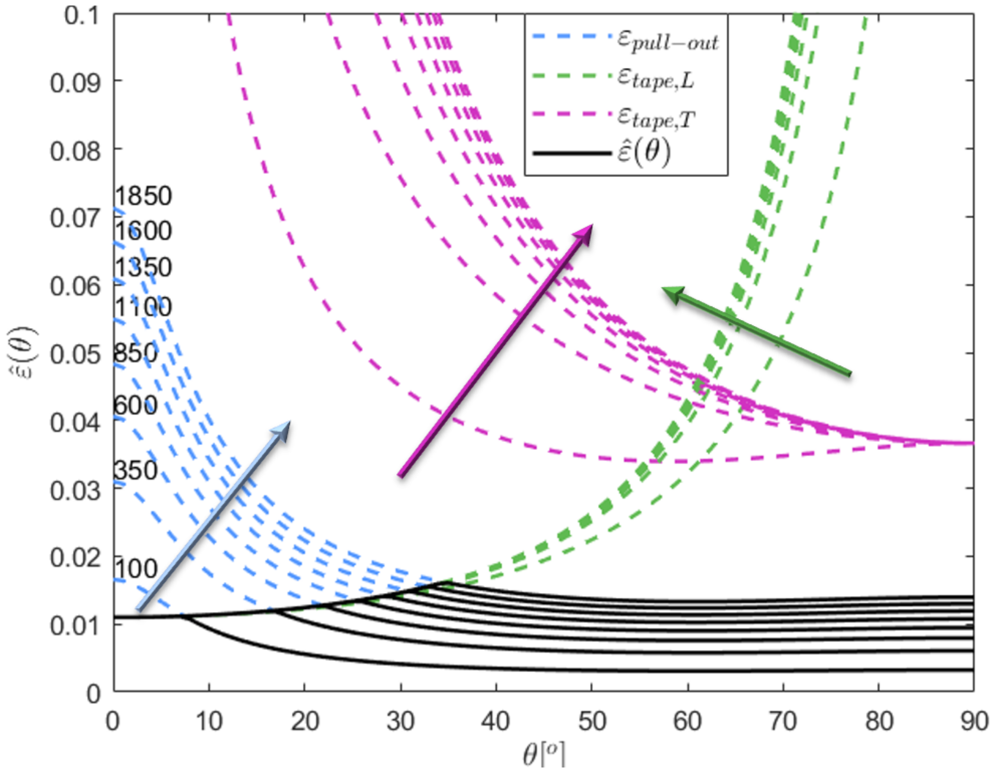

Figure 4.10: Damage initiation strains depending on $\mathcal{G}_{IIC}$ with $t_{tape} = 22.5$ μm and $E_f = 425$ GPa.

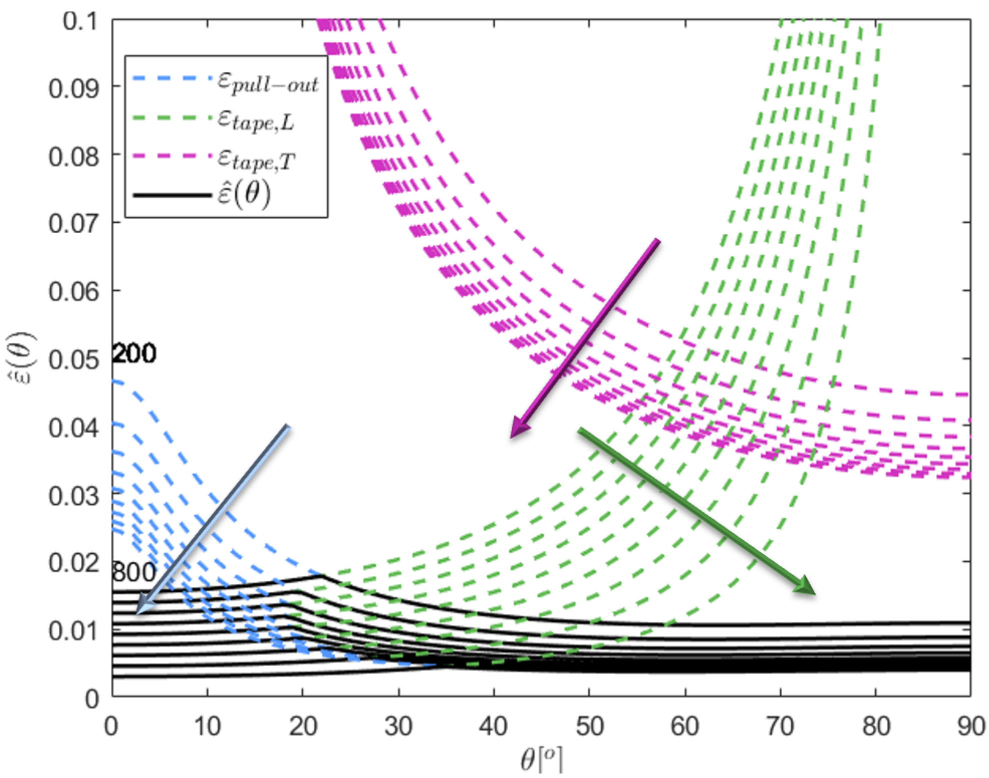

Figure 4.11: Damage initiation strains depending on E_f with least square fit for X_e, $t_{tape} = 22.5$ μm and $\mathcal{G}_{IIC} = 400$ J/m^3.

4.7.3 Fracture modes depending on t_{tape}, $\mathcal{G}_{IIC}$, E_f

The modes of fracture changes depending on t_{tape}, $\mathcal{G}_{IIC}$ and E_f. This can be evaluated for all different angle of tapes to see which fracture mode that is most likely to occur depending on the input parameters. As in Section 4.7.2 the input parameters are the ones found in Table 4.4 and the evaluations are made by varying one parameter while keeping the other two constant. The evaluation for each parameter can be seen in Figures 4.12-4.14. In the figures it can be seen that the most likely fracture mode to occur is pull-out, followed by *HL* which in these figures stands for *longitudinal tape fracture*. It can also be seen that transverse tape fracture never occurs for the simulated laminates, which can also be seen in Figures 4.9-4.11. From Figure 4.12, as well as in Figure 4.9, one can see that when increasing the tape thickness the likeliness of failure by pull-out will increase. However, for a variation inmode II fracture toughness, as seen in Figures 4.13 and 4.10, increasing the fracture toughness instead increases the likeliness of longitudinal tape fracture. As can be seen in Figure 4.14 the most likely mode of failure varies when increasing the fibre stiffness, and for $E_f \approx 425$ GPa the most likely mode of failure is pull-out. This is confirmed in Figure 4.11, in which the fourth full black line from the top belongs to $E_f = 425$ GPa.

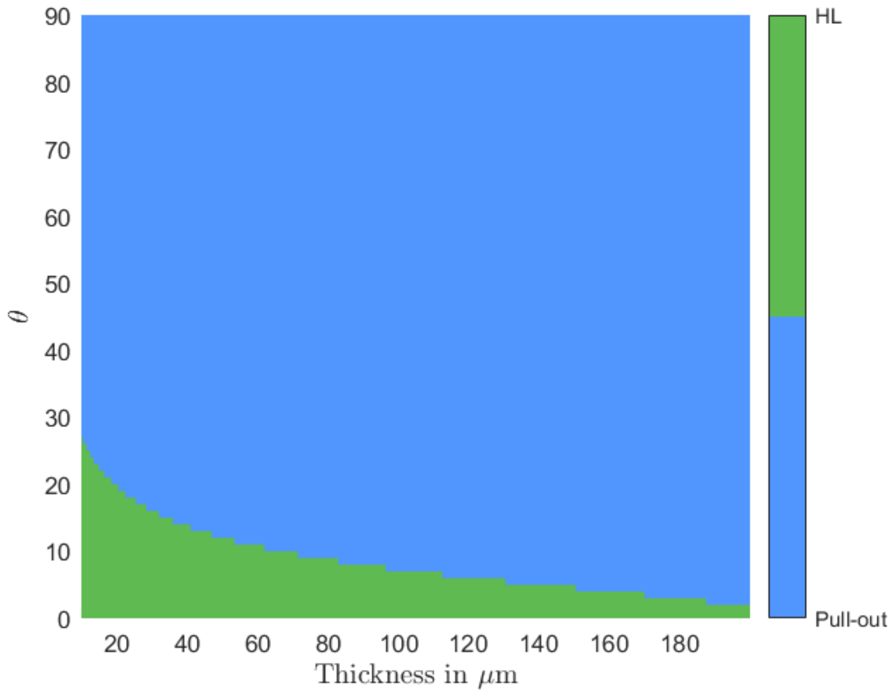

Figure 4.12: Fracture modes for different angles of tape depending on t_{tape} with $E_f = 425$ GPa and $\mathcal{G}_{IIC} = 400$ J/m^3.

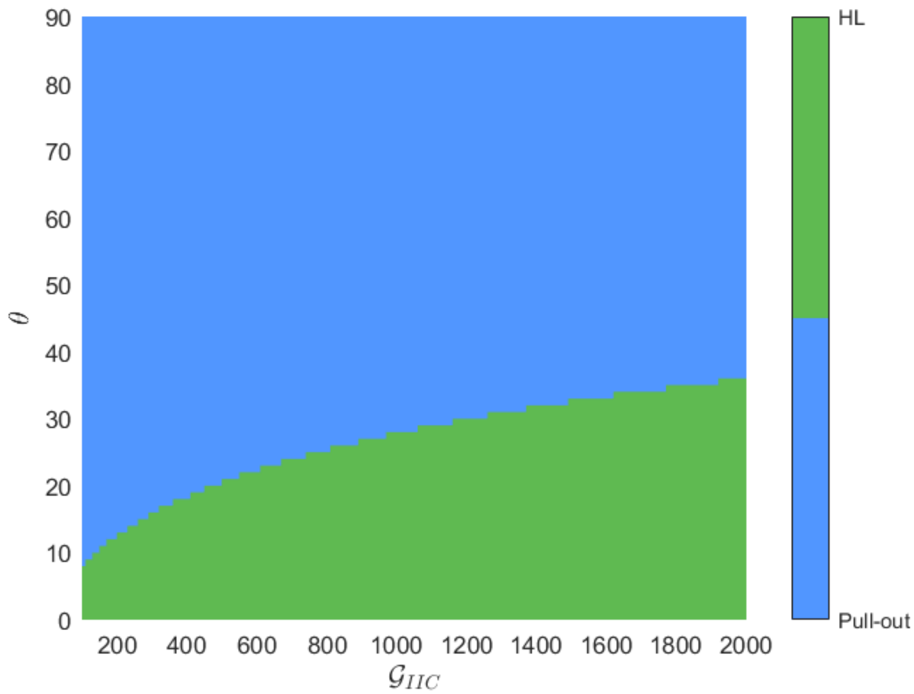

Figure 4.13: Fracture modes for different angles of tape depending on $\mathcal{G}_{IIC}$ with $E_f = 425$ GPa and $t_{tape} = 22.5$ μm.

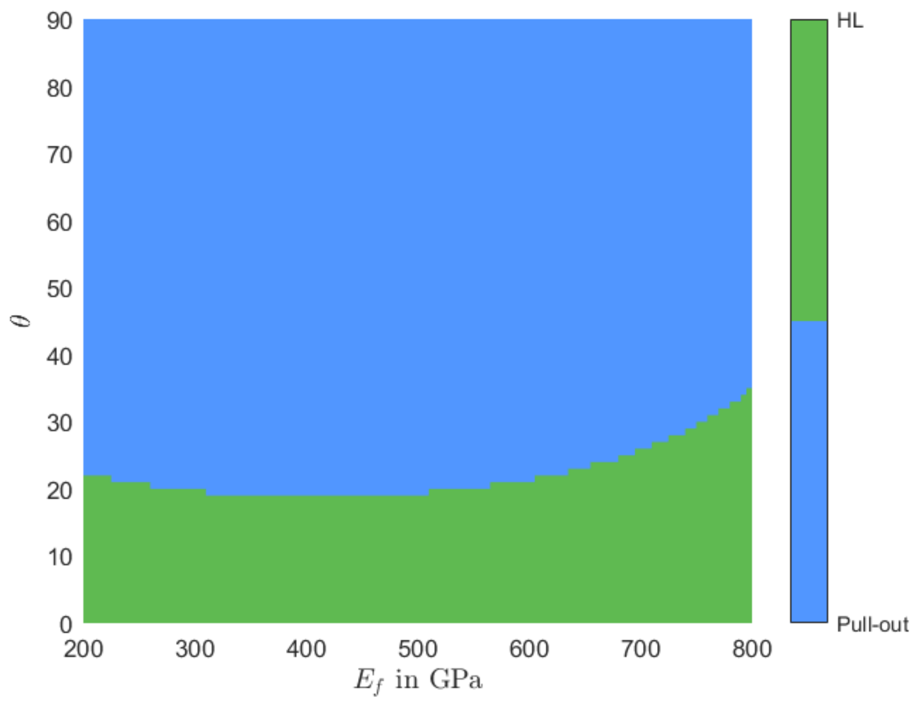

Figure 4.14: Fracture modes for different angles of tape depending on E_f with least square fit for X_e, $t_{tape} = 22.5$ μm and $\mathcal{G}_{IIC} = 400$ J/m^3.

4.7.4 Evaluation of damage initiation strain depending on parameters

To understand how the limiting damage initiation strain depicted as the black lines in Figures 4.9-4.11 change depending a change in thickness, $\mathcal{G}_{IIC}$ or E_f, the change in $\hat{\varepsilon}$ for each case is plotted as a function of these parameters, seen in Figures 4.15-4.17.

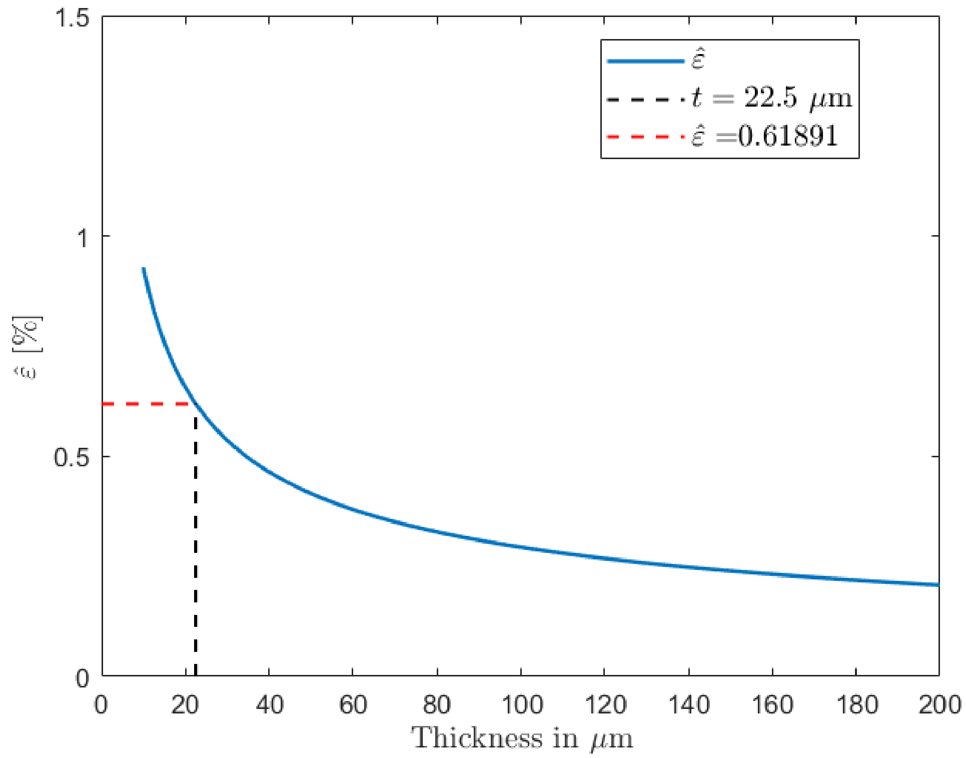

Figure 4.15: Damage initiation strain of the laminate depending on t_{tape} with $E_f = 425$ GPa $\mathcal{G}_{IIC} = 400$ J/m^3.

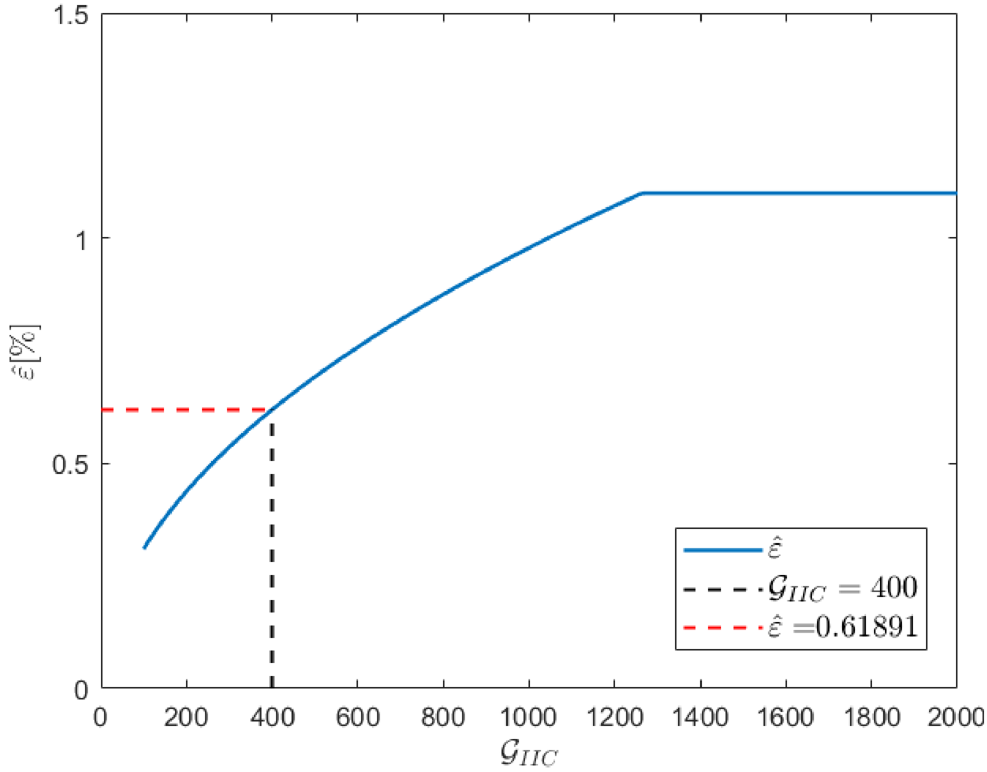

Figure 4.16: Damage initiation strain of the laminate depending on $\mathcal{G}_{IIC}$ with $E_f = 425$ GPa and $t_{tape} = 22.5$ μm.

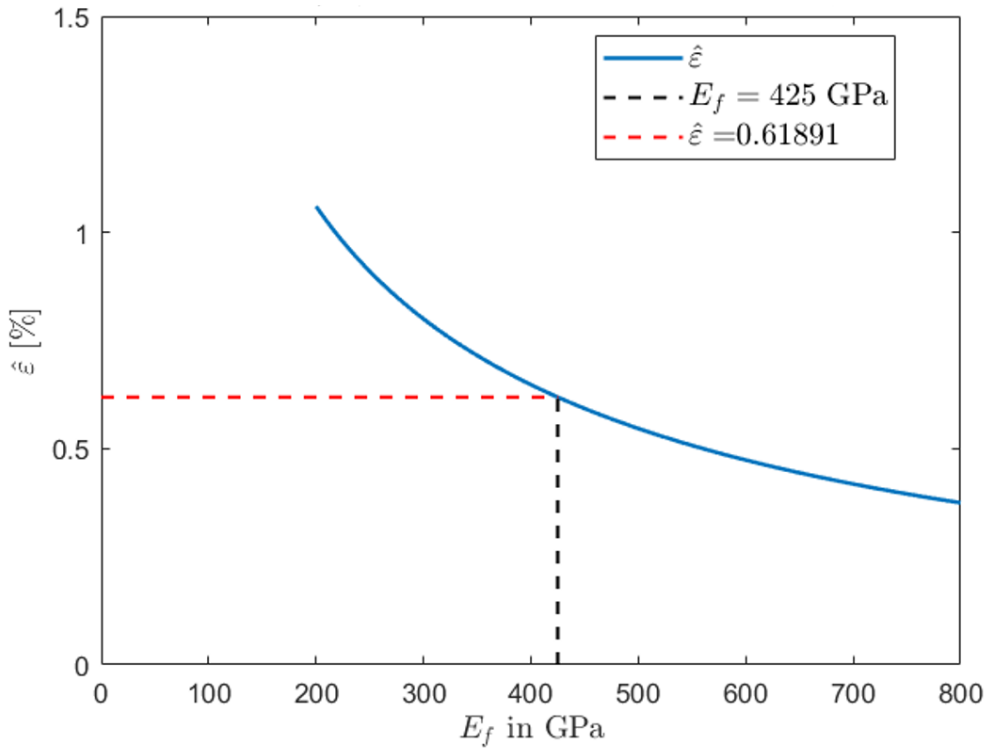

Figure 4.17: Damage initiation strain of the laminate depending on E_f with $\mathcal{G}_{IIC} = 400$ J/m^3 and $t_{tape} = 22.5$ μm.

5

Discussion and conclusion

This chapter contains discussions and conclusions regarding the results obtained from the analytical model as well as the mechanical tests. It also contains a discussion on possible improvements of the analytical model and on future work.

5.1 Comparison with Experimental results

As can be seen in Figure 4.5 the experimental and the analytical results does not exactly match, however the analytical results are within the standard deviation of the experimental results. The fact that the results match this well is encouraging, especially since this is a first try of constructing an engineering model. This proves that we are on the right path, and with a bit of tweaking and with some of the assumptions that are made in the model more closely studied, the accuracy of the model can increase even further. There are several things that may be subject for improvement and further studies to increase the accuracy. First of all, the laminates that were used when performing the mechanical tests were the first laminates manufactured with the tapes that have resin on both sides. Secondly, the laminates size of less than 0.3×0.3 m limited the number of specimen for tensile tests to 12 per laminate, as can be seen in Figure 5.1. Also, since the specimens are cut from different parts of the laminate and the manufacturing process might not result in perfect quality laminates, the mechanical properties may vary between specimen. Thirdly, the experimental tests were performed on two laminates, one with $V_f = 44.1$ % and one with $V_f = 47.7$ %. The results that were used in the comparison with the $V_f = 45.9$ % laminate used in analytical model are the measured average for both plates. Thus, given these inconsistencies in the composites manufacture and test the relatively good agreement between predictions and the test results indicates that the models can predict the performance of UTHMT composites. Furthermore, the computational and experimental results both provide strong indications on what mechanical properties that can be expected for the UTHMT composite laminates in the future.

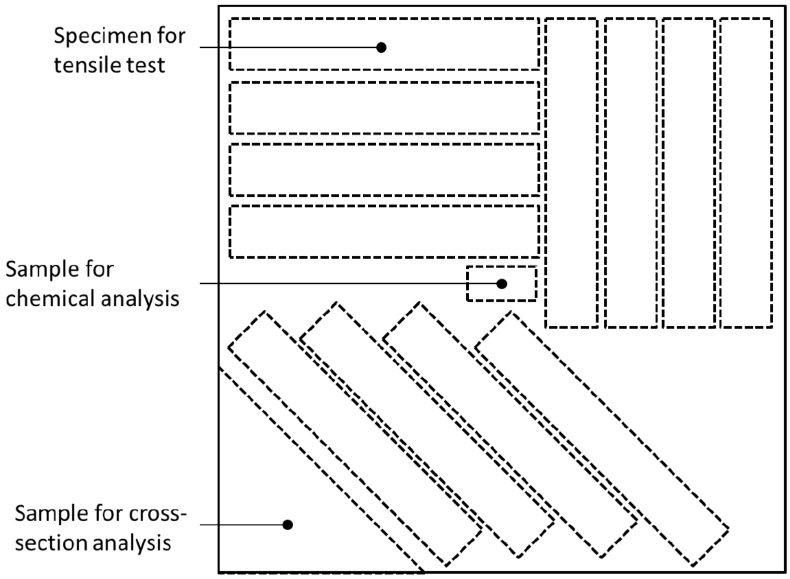

Figure 5.1: How the test specimens were cut from each laminate, from M. Johansen [5].

5.2 Analytical results

The analytical results can be divided into two parts: stiffness and strength.

5.2.1 Stiffness

The accuracy of the stiffness prediction part of the analytical model was first tested using results from the ELT simulations performed by Pimenta et al. [4] and Wan and Takahashi [8]. The similarity between the results of the model and the article indicated that the stiffness prediction yields trustworthy results. This was later confirmed by the simulation of the laminates that were tested experimentally. However, the stiffness prediction part of the model can still be improved somewhat since there are a few assumptions made in the model. These assumptions and possible improvements are discussed in Section 5.3.1.

5.2.2 Strength

The strength prediction indicates that the UTHMT composite laminate has an enormous potential if the manufacturing process can be improved. Even now with imperfect manufacturing of the laminates and lower fibre volume fraction and mode II fracture toughness than targeted, the mechanical properties are most impressing. With conventional carbon fibre composites having first ply failure at $\approx$ 250 MPa, the strength of the UTHMT composite laminate is already almost the double that of conventional continuous CFRP laminates.

As can be seen in Figures 4.9-4.11 the analytical model predicts the strength and fracture mode of the laminate. The fracture mode indicated for the HS40 composite laminate is tape pull-out, which is also confirmed by the fractographic studies made by Mr Johansen [5]. The Figures also indicate that the UTHMT laminate can still be improved by changing the parameters found in Table 4.4, making it possible to customise the laminate for specific use. It takes only a minute to change the fibre volume fraction, tape dimensions, the properties of the carbon fibres and matrix etc. and obtaining a prediction of the mechanical properties, making it possible for quick evaluation of different laminate designs.

5.3 Future work

In this section future work and possible improvements are discussed. The discussions are both regarding possible improvements to the analytical model as well as future work and research that could not be performed within the scope of this project.

5.3.1 Discussion regarding the stiffness prediction

As mentioned in Section 5.1 the manufacturing process needs to be fine-tuned and more specimen must be tested to be able to fully trust the test results. First then can the accuracy of the model be evaluated in detail. There are several assumptions made in the model, and these can be tweaked and further studied. For example the transverse fibre stiffness, which as of now is estimated to be 5 % of the longitudinal fibre stiffness in the ELT prediction. Another assumption is the Poisson's ratio of the fibres ν_f, which is not found in the fibre data sheet for HS40 but instead assumed from a similar carbon fibre found in [6]. The reason that ν_f was not further researched is that the change in laminate stiffness depending on ν_f was evaluated early in the project, using three fibre volume fractions which can be seen in Figure 5.2. The influence of different ν_f deemed to be minor and it was determined that further investigation was to be left for future work.

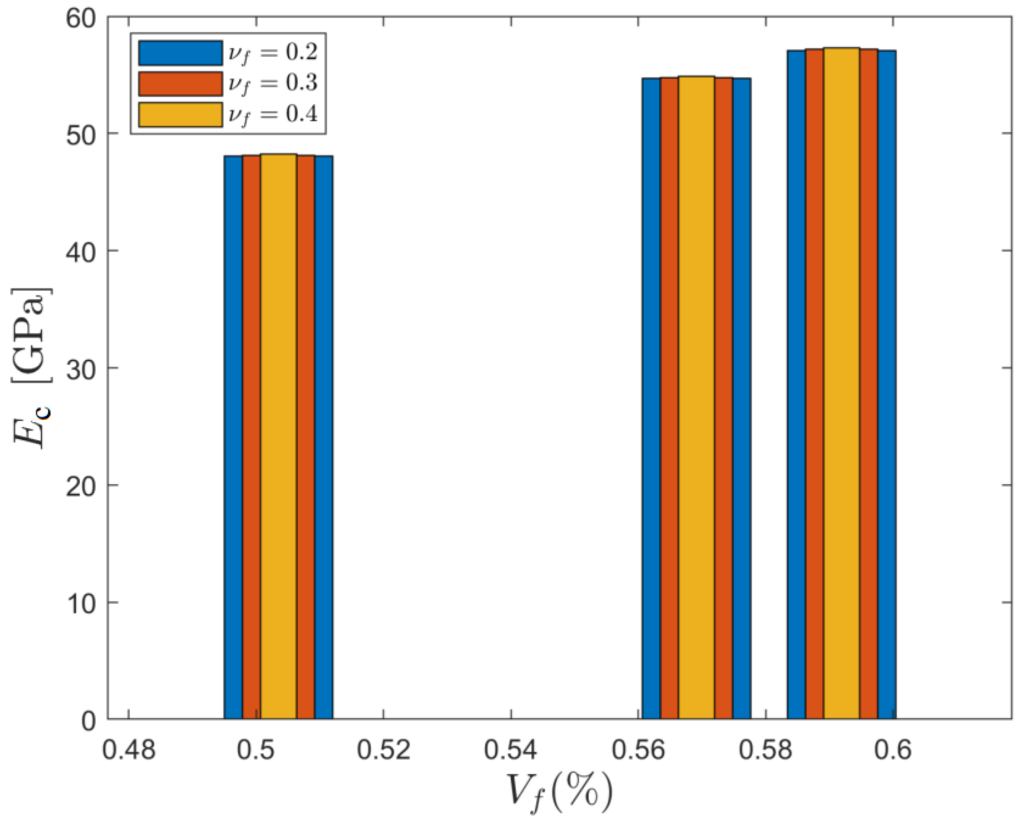

Figure 5.2: Evaluation of change in stiffness for different ν_f.

5.3.2 Discussion regarding the strength prediction

The accuracy of the strength prediction can be tweaked when high quality laminates have been tested and the sample size is larger. Until then it can still be improved concerning the prediction of in-situ shear strength, for more realistic predictions. As for now, the estimation of shear loading is made for linear behaviour. The estimation can also be made for non-linear behavior as can be seen in Figure 3.4, but in the attempt to implement the non-linear behavior it was discovered that the equations regarding the non-linear behaviour were faulty. This could be further researched and implemented in the model for a more realistic prediction of the strength of the laminate.

Increased mode II fracture toughness $\mathcal{G}_{IIC}$ is highly desirable. This can be achieved by different modifications to the process and the matrix material. Firstly, the application of the reactive binder, i.e. the uncured resin, on the tapes should be trimmed to ensure that the entire tape width is covered by the binder. This will increase $\mathcal{G}_{IIC}$ as any dry spots are eliminated. Secondly, the reactive binder itself may be modified to increase $\mathcal{G}_{IIC}$. Modern CFRP pre-preg composites use toughened matrix materials, where the epoxy matrix is toughened by inclusion of small rubber or thermoplastic particles. The 6376 epoxy resin used in the HTA/6337 [16] is toughened in this way, with a resulting high $\mathcal{G}_{IIC} = 1100$ J/m^3.

Other areas of future work is of course the prediction of the mechanical properties of the laminate in regard to compression and shear loading. Through this it would be possible to deliver an analytical model with a failure envelope covering all types of loading. This demands for further literature studies to be performed, new analytical models to be made as well as new laminates to be manufactured and tested experimentally.

Bibliography

[1] Ji B. and Gao H. Mechanical properties of nanostructure of biological materials. *Journal of the Mechanics and Physics of Solids*, 52(9):1963–1990, 2004.

[2] Wang R. Z., Suo Z., Evans A. G., Yao N., and Aksay I. A. Deformation mechanisms in nacre. *Journal of Materials Research*, 16(9):2485–2493, 2001.

[3] Wan Y. and Takahashi J. Tensile properties and aspect ratio simulation of transversely isotropic discontinuous carbon fiber reinforced thermoplastics. *Composites Science and Technology*, 137:167–176, 2016.

[4] Li Y., Pimenta S., Singgih J., Nothdurfter S., and Schuffenhauer K. Experimental investigation of randomly-oriented tow-based discontinuous composites and their equivalent laminates. *Composites Part A: Applied Science and Manufacturing*, 102:64–75, 2017.

[5] Johansen M. Manufacturing and characterisation of ultra-stiff composite material. *Unpublished Master Thesis*, 2019.

[6] Agarwal B.B., Broutman L.J., and Chandrashekhara K. Analysis and performance of fiber composites. 2017.

[7] Wan Y. and Takahashi J. CFRTP mechanical properties simulation by Mori-Tanaka model and equivalent laminate method. *ECCM 2016 - Proceeding of the 17th European Conference on Composite Materials*, (June), 2016.

[8] Wan Y. and Takahashi J. Multi-Scale Internal Geometry Analysis and Mechanical Modeling of. *Conference: 21st International Conference on Composite Materials, At Xi'an, China, Volume: Tsai Award Session, 1*, (August):20–25, 2017.

[9] Pimenta S. and Robinson P. An analytical shear-lag model for composites with 'brick-and-mortar' architecture considering non-linear matrix response and failure. *Composites Science and Technology*, 104:111–124, 2014.

[10] Li Y. and Pimenta S. Development and assessment of modelling strategies to predict failure in tow-based discontinuous composites. *Composite Structures*, 209(May 2018):1005–1021, 2018.

[11] Hashin Z. Failure criteria for unidirectional fiber composites. *J. Appl. Mech 47(2), 329-334 (Jun 01, 1980) (6 pages)*, 1980.

[12] Camanho P.P., Dávila C.G., Pinho S.T., Iannucci L., and Robinson P. Prediction of in situ strengths and matrix cracking in composites under transverse tension and in-plane shear. *Composites: Part A 37 (2006) 165–176*, 2006.

[13] Arteiro A., Catalanotti G., and Reinoso J. et al. Arch Computat Methods Eng (2018). Simulation of the mechanical response of thin-ply composites: From computational micro-mechanics to structural analysis. *J. Appl. Mech 47(2), 329-334 (Jun 01, 1980) (6 pages)*, 2018.

[14] Carlstedt D., Johannisson W., Zenkert D., Linde P., and Asp L.E. Conceptual design framework for laminated structural battery composites. *ECCM18 - 18th European Conference on Composite Materials*, (June), 2018.

[15] Aboudi J., Arnold S.M., and Bednarcyk B.A. Micromechanics of composite materials - a generalized multiscale analysis approach. 1st ed:65–66, 2013.

[16] Asp L.E., Nilsson K-F, and Sjögren A. On transition of delamination growth behaviour for compression loaded composite panels. *International Journal of Solids and Structures 38, 8497-8440*, 2001.